Radiation Physics and Chemistry 165 (2019) 108386

Contents lists available at ScienceDirect

Radiation Physics and Chemistry

journal homepage: www.elsevier.com/locate/radphyschem

Correlation between isothermal Tl and Irsl in K-Feldspars of various types

Ioanna K. Sfampa[a,*], George S. Polymeris[b], Vasilis Pagonis[c], George Kitis[a]

[a] Aristotle University of Thessaloniki, Nuclear Physics Laboratory, 54124, Thessaloniki, Greece
[b] Ankara University, Institute of Nuclear Sciences, Beşevler-Ankara, 06100, Turkey
[c] McDaniel College, Physics Department, Westminster, MD, 21157, USA

ARTICLE INFO

Keywords:
Thermoluminescence
Isothermal thermoluminescence
Infrared stimulated luminescence
Feldspar

ABSTRACT

Feldspars are used as natural dosimeters to date geological and archaeological materials. These minerals are widely used in dosimetric methods of dating using luminescence signals, such as Thermoluminescence (TL), Optically Stimulated Luminescence (OSL) and Infrared Stimulated Luminescence (IRSL). The present work is an effort to compare the Isothermal decay Thermoluminescence signals (ITL) to the IRSL signals from four K-feldspar samples which belong to two different species, namely microcline, and sanidine. The experimental data were fitted by analytical expressions coming from a tunneling recombination model. The results prove that all ITL and IRSL signals can be fitted very accurately with the analytical equations and that only two tunneling components are needed to obtain a high-quality fit. These tunneling components consist of a very fast and intense component, which is followed by an extended slowly decaying component. Significant differences were found between the best-fit parameters of the ITL and IRSL signals, indicating that thermal excitation processes may reach different traps from optical excitation processes in these samples.

1. Introduction

During the past 20 years there has been a significant progress in understanding the luminescence mechanism in feldspars. Both experimental and modeling work has been carried out in order to understand the origin of luminescence signals in these materials, such as Thermoluminescence (TL) (Krbetschek et al., 1997), Optically Stimulated Luminescence (OSL) and Infrared Stimulated Luminescence (IRSL). These phenomena are closely associated with the phenomenon of anomalous fading (AF) effect in dosimetric materials, which is detrimental for applications such as dosimetry and dating (Wintle, 1973).

Over the years, various models have been proposed on the way of explaining the AF effect, such as the tunneling model (Visocekas et al., 1976, 1977; Visocekas, 1985), the localized transition model (Templer, 1986; Tyler and McKeever, 1988) and a model based on competition with radiationless transitions (Chen et al., 2000). The most predominant explanations of AF are based on quantum mechanical tunneling from either the ground or the excited trap's state (Poolton et al., 2002, 2009; Li and Li, 2008; Larsen et al., 2009; Jain, and Ankjærgaard, 2011).

Jain et al. (2012) have described the emission of light in a TL or IRSL experiment on feldspars, using a semi-analytical model based on tunneling recombination within a random distribution of donor-acceptor pairs. According to this model, the stimulation excites the trapping levels and the trapped electrons are raised to a higher energy level. From this level tunneling to the nearest neighbor luminescence center takes place, followed by recombination and light emission. This model was termed as a localized tunneling recombination (LTR) model. Within this model, Kitis and Pagonis (2013) have achieved quantification of this semi-analytical model by developing analytical equations that can describe these luminescence signals. Subsequently, Pagonis et al. (2013) obtained approximate expressions for the time development of nearest neighbor distribution during various types of luminescence experiments. At the same year, Polymeris et al. (2013) investigated the possibility of using TL for the structural characterization of ten K-feldspar samples. They have found a relation between TL sensitivity and individual K-feldspar structure. The properties of the samples used by these authors make them ideal for investigating basic TL, OSL and IRSL properties, in addition to possible corresponding correlation (Sfampa et al., 2015; Kitis et al., 2016b).

Moreover, Correcher et al. (2000) made a thorough research over a K-feldspar called adularia using luminescence techniques combined with XRD measurements. These authors found changes in the shape of the glow curve after different thermal pre-treatment, which was attributed to thermal alkali self-diffusion through the twinning interfaces of the lattice, tilting of the Al-Si crankshafts and partial phase changes.

* Corresponding author.
E-mail address: isfaba@physics.auth.gr (I.K. Sfampa).

https://doi.org/10.1016/j.radphyschem.2019.108386
Received 16 May 2019; Received in revised form 20 June 2019; Accepted 25 June 2019
Available online 27 June 2019
0969-806X/

A few years after, Garcia-Guinea et al. (2003) used the thermoluminescence emission spectra in order to study volcanic sanidine and they concluded that the characteristic 380 nm spectral band of sanidine is may linked to thermal alkali self-diffusion mechanisms and the anomalous fading of thermoluminescence signal. They also refer in their paper that this trend to minimize the total free energy from a metastable disordered lattice of sanidine to other re-ordered K-feldspar phase is through the spontaneous coherence strain of the structure and may also include local strain caused by cluster phases of Na-feldspars.

The main objective of the present study is to use the analytical expressions of Kitis and Pagonis (2013) to describe isothermal TL (ITL) and IRSL signals from several K-feldspar samples, as well as to quantitatively compare those signals. At present, it is unknown if thermal and infrared stimulations of feldspars access the same luminescence trap and whether the tunneling recombination takes place via the same pathways. These commonly made assumptions are tested in this study. Furthermore, in the framework of the LTR model by Jain et al. (2012) these two phenomena are described by the same main analytical expressions; however, the expression for the stimulation probability differs. The present work aims to investigate their correlation and mainly to examine if they are expressed through the same experimental values of the model parameters.

2. Experimental procedure

2.1. Materials

The samples used in this study include a selection from the feldspars used by both Polymeris et al. (2013) and Sfampa et al. (2015); these are listed in Table 1. Four naturally occurring K-feldspars from igneous rocks of Northern Greece were studied. The K-feldspars were separated from mafic and felsic minerals with the use of Franz (model L-1) magnetic separator and Sodium Polytungstate (SPT) heavy liquid, respectively. X-ray powder diffraction (XRPD) has been used in order to (a) identify the purity of K-feldspars, (b) estimate the unit cell parameters, as well as, calculate refinements, using the CHEKCELL software (Laugier, Bochu), (c) calculate the probability Σt_1 ($t_{10}+t_1m$) of an Al-cation occupying one of the T_1 sites using the Kroll and Ribbe equation (1987), and (d) classify the samples and divide them into different groups. According to the XRPD patterns of the examined samples, they are divided into three groups-types, namely sanidines, orthoclases, and microclines. The probability Σt_1 has the lowest values for sanidine and the highest values for the samples of the sanidine group. More details about the XRPD results are found in Polymeris et al. (2013). Two samples from the sanidines and two samples from the group of microclines have been selected. Structural classification of K-feldspars is summarized by Deer et al. (1992) and spectral information from feldspars relevant for luminescence dating was previously presented by Krbetschek et al. (1997).

2.2. Apparatus

Luminescence measurements were performed by a Risø TL/OSL reader (model TL/OSL DA 15), equipped with a $^{90}Sr/^{90}Y$ beta particle source, delivering a nominal dose rate of 0.075 Gy/s and a 9635QA photomultiplier tube. The detection optics consisted of a combination of the 2 mm Schott BG 39 and the 4 mm Corning 7-59 (known as the blue filter pack) (Şahiner et al., 2017); this former combination was used, since it consists of the optimum filter combination for the cases of feldspar luminescence using Risř TL/OSL reader models TL/OSL DA 15 and DA 20. The measurements were executed in a nitrogen atmosphere with a heating rate of 2 °C/s, to avoid significant temperature lag, and the samples were heated up to the maximum temperature of 500 °C. For IRSL, the stimulation wavelength is 875 (± 40) nm and the maximum power delivered at the sample was ~135 mW/cm^2.

Table 1
K-feldspar samples studied in the present work.

Sample	Kf_s	Species Unit cell volume (A^3)	Σt_1
BAL-2	Sanidine	706.47 ± 0.37	0.58 ± 0.02
SAM-3	Sanidine	708.55 ± 0.28	0.60 ± 0.02
VRS-8	Microcline	719.21 ± 0.37	0.88 ± 0.02
KST-4	Microcline	720.51 ± 0.40	1.01 ± 0.03

2.3. The experimental protocols

The experimental procedure is divided into two different protocols. Three aliquots of each sample were prepared, of almost 7mg each, in order to ensure the reproducibility of the results. Protocol #1 is termed hereafter as the post ITL-IRSL protocol, while Protocol #2 is termed hereafter as the post IRSL-IRSL protocol.

- Step 0: Test dose and TL measurement up to a temperature T = 500 °C at 2 °C/s, to empty the traps and measure the initial sensitivity of the sample.
- Step 1: Test dose
- Step 2: Isothermal Decay (ITL) measurement at a temperature T_i for 500 s for Protocol #1, and Continuous-wave IRSL (CW-IRSL) measurement at a temperature T_i for 500 s for Protocol #2.
- Step 3: CW-IRSL measurement at a temperature (T_i -10) °C for 500 s,
- Step 4: TL measurement up to a temperature T = 500 °C at 2 °C/s, to measure the remnant-TL signal (RTL).
- Step 5: Repeat steps 1–4 for a new temperature T_i , in steps of 10 °C
- Step 6: Test dose and TL measurement up to a temperature T = 500 °C at 2 °C/s, to measure the final sensitivity of the sample.

The maximum temperatures T_i used for ITL and IRSL decays were dependent on the position of the temperature T_m of maximum intensity for the main dosimetric peak of the sample. The value of T_m is different for the four samples, as shown in Fig. 1. For the case of sample BAL-2, the range was chosen as T_i = 40-200 °C, for KST-4 and VRS-8 samples the range T_i = 40-130 °C and finally for SAM-3 sample T_i = 40-170 °C. The main rationale behind selecting these temperatures is to measure both IRSL and ITL signals at temperatures just below T_m. It is important to highlight the fact that step 3 is the same for both protocols, in order to be able to compare the same type of signals. The temperatures selected on that step are connected with the temperatures T_i used on step 2 and specifically they are (T_i -10 °C). The aim of that is to minimize any further thermal excitation during the IRSL measurement and keep that signal as clearer as possible.

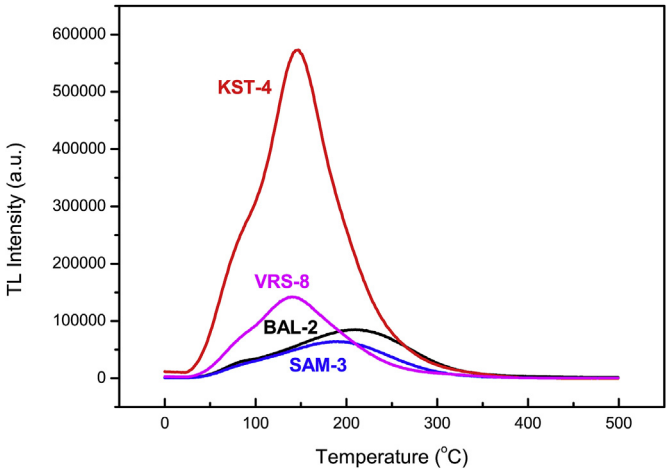

Fig. 1. Typical glow curves of the four samples used in the experiments.

Both the ITL and CW-IRSL protocols run in a single aliquot, since it was recently established by Pagonis et al. (2015) that the luminescence signals from the same potassium feldspars do not become sensitized when they undergo cycles of irradiation and heating. In the framework of both protocols of this paper, additional sensitivity tests were also applied two more times, in steps 0 and 6 of the protocol. The results verified once again the excessive stability of these materials to successive irradiation–TL readout cycles and almost negligible sensitivity changes.

3. Method of analysis

The experimental data were analyzed by applying a curve-fitting approach based on the analytical equations presented below. In the computerized curve deconvolution analysis of ITL and CW-IRSL curves, the goodness of fit was tested by the figure of merit (FOM) of Balian and Eddy (1977). Microsoft Excel along with the *Solver* add-on feature (Afouxenidis et al., 2012) has been utilized for all curve fittings.

Both IRSL and ITL curves were analyzed using the analytical solutions of the set of differential equations in the localized transition which were derived by Kitis and Pagonis (2013). The analytical expressions used in the present paper are the following:

$$I(t) = \frac{C[F(t)]^2}{1 + z\mathcal{A}t} \cdot \exp\left(-\rho'[F(t)]^3\right) \quad (1)$$

$$F(t) = \ln(1 + z\mathcal{A}t) \quad (2)$$

where C is a constant related to the initial concentration of trapped electrons and the quantity $\mathcal{A}$ (s^{-1}) represents the stimulation probability for either the ITL or the IRSL stimulation process. The stimulation probability can also be described as $\mathcal{A} = 1/\tau$, where τ is the characteristic time, typical for each stimulation mode, and $I(t)$ represents the intensity of the signal as a function of time. The time parameter in the case of ITL represents the duration of the isothermal experiment, while in the case of the IRSL signal it represents the optical bleaching time.

In the above-mentioned equation, ρ' is the dimensionless concentration of charge carriers and $z = 1.8$ is a constant numeric value. The stimulation probability for the IRSL process is given by $\mathcal{A} = \sigma \cdot I_o$, where σ is the IRSL cross-section, and I_o is the corresponding IR stimulation intensity. In the case of the ITL experiments $\mathcal{A} = s \cdot exp(-E/kT)$, where T is the constant temperature, E the activation energy, s is a frequency factor and k is the Boltzmann constant.

Moreover, instead of Eq. (2), the empirical modified form,was used. This empirical modification is based on the requirement that the intensity of the normalized Eq. (1) should be unity for t = 0. Nevertheless, this problem is restricted to a few seconds at the beginning of the stimulation, while its impact becomes negligible for long stimulation times; moreover, the modified equation (2a) has already been successfully applied in previous cases (Polymeris et al., 2018a; Angeli et al., 2019).

$$F(t) = \ln(e + z\mathcal{A}t) \quad (2a)$$

An example of a component-resolved ITL decay curve is shown in Fig. 2a. It was found that a unique tunneling component is required to obtain a high-quality fit. The use of one tunneling component for the cases of ITL signals stands in good agreement to previous related studies in Durango apatite (Sfampa et al., 2014). The FOM value for the analysis of all samples was less than 2%.

Similarly, it was found that the IRSL decay curves measured in the present study consist of two tunneling components, a very fast and intense first component (C1), followed by an extended slowly decaying second component (C2). The use of two tunneling components for the cases of IRSL signals stands in agreement to previous related studies in feldspars (Pagonis et al., 2014; Sfampa et al., 2015; Kitis et al., 2016b; Şahiner et al., 2017; Angeli et al., 2019). Fig. 2b shows the results of the component analysis for a typical IRSL decay curve. The FOM values for the analysis of all samples were less than 2.7%, which is considered as truly satisfied result.

4. Results

4.1. General behavior of the ITL, IRSL signals

The ITL and IRSL signals were investigated by using normalized curves over the maximum initial intensity at stimulation time t = 0. The behavior of these, normalized ITL and IRSL signals measured in the two protocols for sample BAL-2, as a function of time are presented in Fig. 3. This normalization was performed in order to investigate possible changes taking place in the shape of the various ITL and IRSL curves. The normalized curves show that with an exception of the first ITL curves which were measured at low stimulation temperatures, within the range 30-50°C, all the other curves coincide for the same stimulation mode. This feature indicates that the shape of the ITL curves is independent on the stimulation temperature, unlike what is usually expected for a strong dependence of the ITL over the decay temperature. Similar behavior was monitored for all four samples of the present study. This behavior of the signals is typical of tunneling recombination processes, and has been reported in both natural and synthetic dosimetric materials, in the past. Specifically, a similar behavior was reported in our previous study of isothermal TL curves in the same material (Sfampa et al., 2015). The same method of analysis has been used also for the ITL of synthetic materials by Kitis et al. (2016a), as well as the thermally assisted OSL (TA – OSL) curves of both apatite and quartz samples measured at the isothermal mode (Kitis et al., 2013b and Polymeris et al., 2018b respectively). In all cases, the results indicate the same trend as those in the present study.

The results in Fig. 3 provide strong qualitative experimental evidence that the processes involved include mainly tunneling recombination, which has been also referred by Garcia-Guinea et al. for the case of volcanic sanidine. The differences in the shapes of the normalized signals for the low stimulation temperatures (30°C-50°C) could be associated with unstable shallow trap contributions, as Fig. 1 reveals; nevertheless, further investigation is required for the verification of this latter statement.

4.2. Results from protocol #1: ITL and post ITL-IRSL (pITL-IRSL) signals

Fig. 4 shows the results of analyzing the ITL signals using equations (1) and (2a), where the characteristic time constant $\tau = 1/\mathcal{A}$ for the ITL process is shown for the unique ITL component as a function of the stimulation temperature for all 4 samples. For all samples the τ value decreases abruptly after the first three initial stimulation temperatures. In the case of the microcline samples, the τ value increases after 70°C, reaching a plateau and finally the initial τ value is retrieved at higher temperatures. For the sanidine samples, the τ values reach a plateau and remain stable at higher temperatures. The lifetime averages calculated from the plateau regions are $\tau_{BAL\text{-}2} = (0.52 \pm 0.056)$ s (representing the mean value of the last 14 data points with uncertainty of 10%), $\tau_{SAM\text{-}3} = (1.03 \pm 0.053)$ s (for the last 11 data points with uncertainty of 5%) and finally for the VRS-8, $\tau_{VRS\text{-}8} = (1.014 \pm 0.1)$ s (for the last 7 data points with uncertainty of 9.8%).

The dimensionless concentration of charge carriers (ρ') for the case of the ITL procedure is presented in Table 2. All the samples show an almost stable value of ρ' with an uncertainty less than 8%, except for the sample VRS-8 which has a larger uncertainty of around 15.4%, with the value ranging between 3.3 and 15.6 10^{-3}.

The second part of protocol #1, including the pITL-IRSL signal, is measured on step 3. The values for the corresponding fitting parameters are presented in tabulated form (refer to Table 2). The first tunneling component displays a stable $\tau = 0.18$s value for sample BAL-2, $\tau = 0.48$s for sample SAM-3, $\tau = 0.57$s for KST-4 and $\tau = 0.62$s for VRS-8. In other

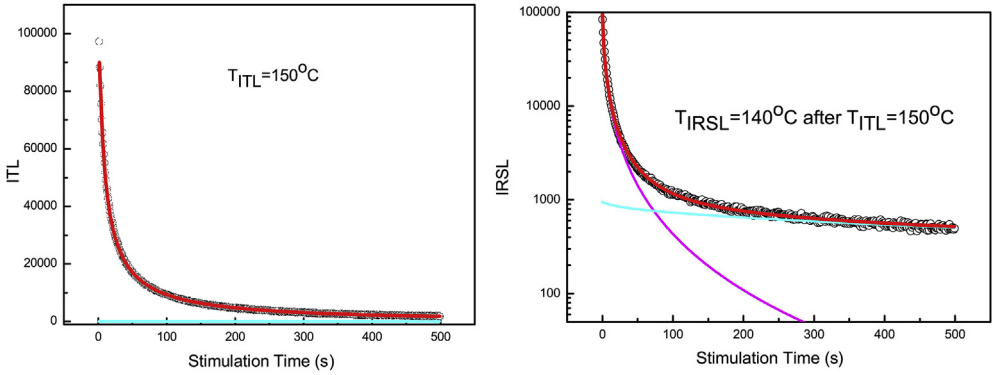

Fig. 2. Fig. 2: (a) Component-resolved analysis example of an ITL and **(b)** an IRSL decay curve for the sample BAL-2.

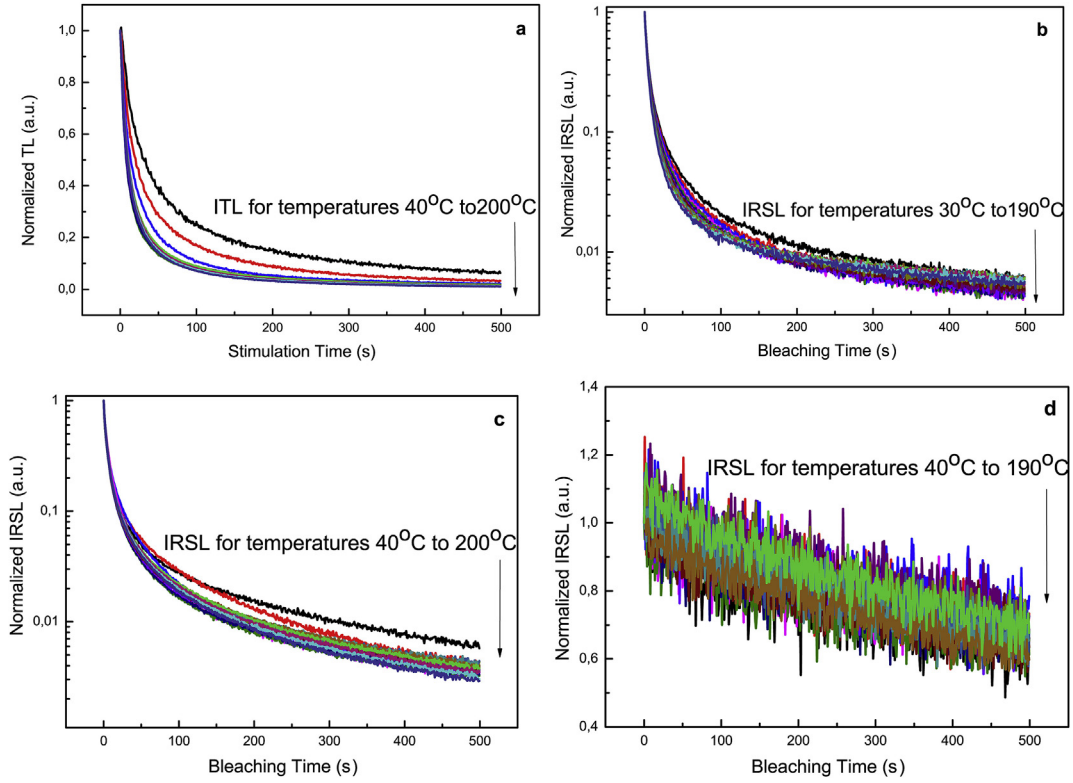

Fig. 3. Sample BAL-2: (**a**) ITL measurements according to the Protocol #1 for T_i = 40°C-200°C, (**b**) IRSL measurements carried out after the ITL in (a), pIR-IRSL. These are measured with Protocol #1 and for T_i = 30°C-190°C, (**c**) initial IRSL measurements carried out with Protocol #2 and for T_i = 40°C-200°C, (**d**) pIR -IRSL measurements carried out after initial IRSL in (c) with Protocol #2 and for T_i = 40°C-190°C.

words, the τ values are lower for the cases of pITL-IRSL signals for all four samples, compared to those of the (previous) ITL signals. On the other hand, the dimensionless concentration of charge carriers ρ′ for the case of the pITL-IRSL procedure results into values ranging between 8.5 and 17.3·10^{-3} namely higher than the corresponding of ITL signals. All fitting parameters are also presented on Table 2 and yield uncertainties less than 5%.

For all cases of the IRSL signals, a second slow component is required in order to achieve better fittings. An example of that is presented on Fig. 2b. Lifetimes for these slow components are in the range 20-50s, while values of ρ′ range between 0.0004 and 0.002 for the microcline samples, and from 0.001 to 0.008 for the sanidines. The large uncertainties in these values may be due to the fact that the experimental background contributes to the luminescence signal, and especially to the second component.

4.3. Results from protocol #2, IRSL and post IR-IRSL (pIR-IRSL) signals

The second protocol consists of two IRSL measurements. Each initial IRSL curve was once more fitted by two tunneling components. The first one is the dominant component, with the corresponding fitting parameters shown in Table 2. These initial IRSL measurements present τ values around τ = 0.25s for BAL-2 and τ = 0.73s for SAM-3, while for the microcline samples the corresponding values were yielded as τ = 0.95s for KST-4 and τ = 0.86s for VRS-8. Once again, the corresponding values for the fitting parameters are also presented in Table 2. The dimensionless concentration of charge carriers ρ′ for the case of the initial IRSL measurements present an almost stable value ranging between 6.1 and 13.8 10^{-3}. Similarly to the previous cases, the errors of the best fitting parameters can be considered as very low. For the notable exception of the ρ′ value of KST-4, where the uncertainty is almost 19%, it is our belief that this difference may be attributed to the accuracy and precision of the experimental data. Concerning the second (slow)

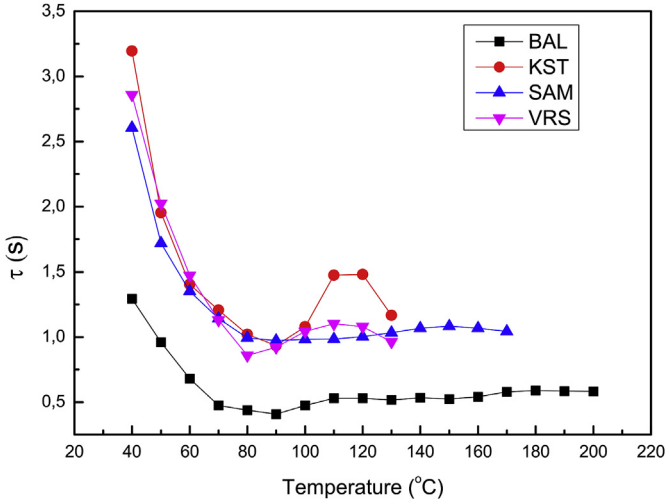

Fig. 4. The dependence of the lifetime recombination parameter, τ, on the stimulation temperature for the unique component of ITL curves of step 2 in protocol #1.

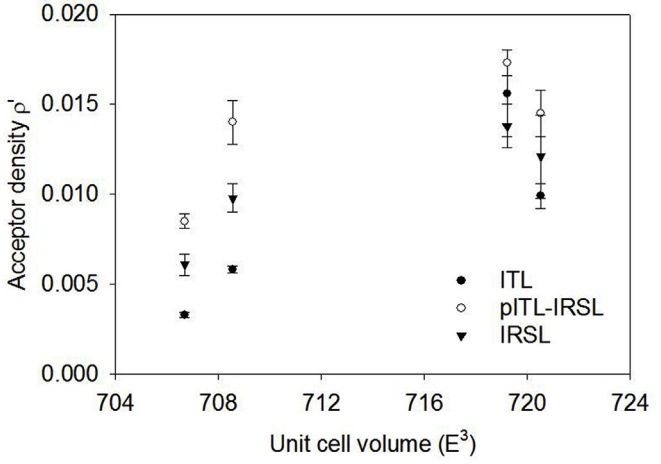

Fig. 5. The values of ρ′ is almost similar between the different procedures and it slightly raises as a function of unit cell volume.

Table 2
The results for the τ and ρ′ values yielded after the fitting analysis.

		Sanidines	
		τ	ρ' (x 10^{-3})
BAL-2	**ITL** (40-170°C)	FIG.4	3.3 ± 0.14 (4%)
	pITL-IRSL (C1) (60-190°C)	0.18 ± 0.014 (7.8%)	8.5 ± 0.41 (5%)
	IRSL (C1) (60-190°C)	0.25 ± 0.018 (7.6%)	6.1 ± 0.6 (9.8%)
SAM-3	**ITL** (60-170°C)	FIG.4	5.8 ± 0.19 (2.4%)
	pITL-IRSL (C1) (40-160°C)	0.48 ± 0.011 (2.3%)	14 ± 1.2 (8.5%)
	IRSL (C1) (40-160°C)	0.73 ± 0.014 (2.1%)	9.8 ± 0.8 (8.2%)
		Microclines	
KST-4	**ITL** (40-120°C)	FIG.4	9.9 ± 0.7 (7.1%)
	pITL-IRSL (C1) (30-120°C)	0.45 ± 0.043 (9.5%)	14.5 ± 1.3 (9%)
	IRSL (C1) (30-120°C)	0.95 ± 0.055 (5.8%)	12.1 ± 2.3 (18.9%)
VRS-8	**ITL** (40-120°C)	FIG.4	15.6 ± 2.4 (15.4%)
	pITL-IRSL (C1) (30-120°C)	0.62 ± 0.063 (10.1%)	17.3 ± 0.73 (6.1%)
	IRSL (C1) (30-120°C)	0.86 ± 0.1 (11%)	13.8 ± 1.2 (8.7%)

component in the IRSL signal, τ has again rather high values, with a maximum of τ = 300s, for sample SAM3, while ρ′ is almost stable around 0.0002.

The final step in the protocol includes again an IRSL measurement. As it becomes obvious from Fig. 3d, this IRSL signal presents a very low signal and poor statistics; therefore curve-fitting analysis was not attempted.

5. Discussion

A first, notable result from the curve-fitting analysis in the present study deals with the stability of the ρ′ parameter for each stimulation, throughout the entire temperature region, for each sample. According to the initial model by Jain et al. (2012), the dimensionless density parameter ρ′ should remain constant, and this is in agreement with the experimental data not only in this study but also in previous studies (Şahiner et al., 2017). Moreover, the values of this parameter stand in excellent agreement with the values suggested by Pagonis et al. (2014, 2015). However, the stability of the τ parameters was not anticipated and arises from the independence of the ITL and IRSL decay curves, mostly on the stimulation temperature.

Both protocols include an initial stimulation (either using ITL or initial IRSL) and a second IRSL measurement. Therefore, at first, one can compare the fitting parameters of the two initial stimulations of each protocol. According to Fig. 4 and Table 2, ITL decay curves indicate higher τ values than those of the (initial) IRSL decay curves. A higher value of τ parameter, in conjunction with the practically constant dimensionless parameter ρ′, indicates that the recombination process requires gradually more time since the electrons recombine with more distant holes at higher stimulation temperatures. Regarding the values of the dimensionless concentration of charge carriers ρ′, ITL decay curves indicate lower values than those of the (initial) IRSL decay curves. The corresponding values of the fitting parameters indicate that according to the LTR model, the tunnelling recombination during ITL takes place from different pathways than in the case of the tunnelling recombination during stimulation using infrared radiation. Moreover, ITL stimulation takes more advantage of the most distant pairs of donors and acceptors than the corresponding initial IRSL signal, by consuming more proximal pairs by recombination from around the excited state of the trap. At the same time, ITL indicates lower values of the dimensionless concentration of charge carriers ρ′. It was suggested that the value of this parameter could be related to the energy and mobility of the band tail states; the lower these values get, the more disconnected these band tails are.

Following the same rationale, one can compare the fitting parameters of the two secondly stimulated IRSL signals. Unfortunately, this was not possible, as the pIR-IRSL decay curves were not fitted, due to their faint intensity. Nevertheless, according to the values presented in Table 2, the fitting parameters of the pITL-IRSL of protocol #1 could be compared to the corresponding parameters of the initial IRSL of protocol #2. Once again, the comparison indicates differences in both values of all four samples. This latter conclusion indicates that the tunnelling recombination depends strongly on the sequence of the stimulations. It becomes obvious that when two sequential stimulations take place, the initial stimulation gets consuming more proximal pairs by recombination from around the excited state of the trap. This feature does not depend on the type of stimulation (thermal, optical or composite). These results stand in good agreement with the results of Şahiner et al. (2017).

Regarding the τ values, for each stimulation modulus, the sample BAL-2 gets the lowest values among the four feldspars of the present study. The values yielded for the other three samples are similar, as Table 2 indicates. Moreover, the values of the ρ′ parameter for each stimulation modulus indicates grouping, being quite low and similar for both sanidine samples, and larger for the microcline samples VRS8 and KST-4. The grouping of the ρ′ parameters can be explained in terms of

unit cell volume; microclines indicate the largest unit cell volumes, while the sanidines the smallest unit cell volumes. Consequently, the concentration of donor-acceptor pairs depends strongly on the unit cell volume and the Σt_1 (see Fig. 5). This latter feature can also be supported by Polymeris et al. (2013), where the microclines indicate the maximum integrated TL intensity among all samples. Basically, the present study provides hints for the possibility of a straightforward correlation between the values of the dimensionless concentration of charge carriers ρ', macroscopically obtained after curve-fitting of IRSL/ITL signals within the LTR model of Jain et al. (2012) using the equations of Kitis and Pagonis (2013) and the microscopically estimated structural characteristics of K-feldspars, such as the volume of the unit cell as well as the probability of Al cation to occupy one of the T1 sites (Σt_1). Further work is required in this direction, using more stimulation modulus (ITL, IRSL, pIR-IRSL, etc) using all K-feldspar samples.

Moreover, the experimental data may be used to obtain a numerical estimate of the dimensionless acceptor density ρ', which is defined by:

$$\rho' = 4\pi\rho\alpha^3/3 \tag{3}$$

where ρ is the actual acceptor number density (number of acceptors per m^3), and a is the tunneling length of the wavefunction.

Poolton et al. (2002a, b) considered the simplest possible electron-trapping defect in a solid, which consisting of a single electron trapped by a single positive charge located at the center of the defect. These authors discussed how this simplified model would be consistent with the crystal structure of a *Na*-feldspar crystal $NaAlSi_3O_8$, shown in Fig. 2b of Poolton et al. (2002a). By using this simple hydrogenic model, they were able to calculate the energy difference between the ground state and the excited state as E = 1.48 eV, in close agreement with the experimental values in the range E = 1.41 1.47 eV from IRSL experiments.

These authors considered tunneling processes taking place from either the ground state of their hydrogenic system, or via transitions involving the first excited state. They concluded that in freshly irradiated samples, recombination takes place mostly through tunneling from the ground state of the electron trap, with holes trapped within the unit cell.

In samples which are not freshly irradiated, Poolton et al. (2002a, b) concluded that tunneling recombination will take place predominantly from the excited state, at much larger distances, and at least one-unit cell away from the electron trap.

Poolton et al. (2002a, b) evaluated the wavefunction for the ground state of the hydrogen-like Na atom, given by:

$$\psi = Aexp\left(-\frac{r}{\alpha}\right) \tag{4}$$

The tunneling length a represents the distance r at which the wavefunction drops to 1/e = 37% of its maximum value, and is $a \approx 1.6$ Å. Fig. 2a in Poolton et al. (2002a) shows that the maximum tunneling recombination probability occurs near this tunneling distance a.

We can also estimate the effective density ρ, by using our experimental unit cell volumes in Table 1. The average unit cell volume for the four feldspar samples is $V_s = 713.7$ Å^3, and we assume one Na acceptor atom per unit cell, as shown in the crystal structure in Fig. 2b of Poolton et al. (2002a).

The effective charge density is then ρ = (1 acceptor/V_s) = $1.4 \times 1027\, m^{-3}$ and from Eq. (3) we obtain:

$$\rho' = \frac{4\pi\rho\alpha^3}{3} = \frac{4\pi(1.4 \times 10^{27}m^{-3})(1.6 \times 10^{-10}m)^3}{3} = 0.024 \tag{5}$$

This value of ρ' is of the same order of magnitude as the average value $\rho' = 0.011 \pm 0.004$ obtained for all ρ' values in Table 1. It is also in agreement with the average value of $\rho' = 0.002$ - 0.01 obtained by Pagonis et al. (2014) by analyzing the CW-IRSL signals from a suite of 23 feldspars of different origin. In addition, this estimate of ρ' is of the same order of magnitude as the values of ρ' obtained by Kitis et al. (2016) from analyzing both TL data and CW-IRSL signals in feldspars.

In the case of TL, we might expect that the effective tunneling length a may be somewhat larger, due to thermally assisted processes in the crystal (Poolton, 2002b), and also due to tunneling from the excited state of the defect.

6. Conclusions

- The normalized ITL and IRSL curves (Fig. 3) coincide, independently on the stimulation temperature. This is considered a typical behavior for tunneling recombination processes at elevated temperatures.
- The difference in the shapes of the normalized IRSL curves for the low stimulation temperatures $T_i = 40^oC$-50^oC could be associated with unstable shallow trap contributions.
- All fitting analysis with equation (1) yielded very good results.
- Significant differences were found between the parameters describing the ITL and IRSL signals, indicating that thermal excitation processes may be reaching either different traps or different recombination pathways from optical excitation processes in these samples.
- The present study provides hints for the possibility of a straightforward correlation between the values of the dimensionless concentration of charge carriers ρ', macroscopically obtained after deconvolution of IRSL/ITL signals within the LTR model of Jain et al. (2012) using the equations of Kitis and Pagonis (2013) and the microscopically estimated structural characteristics of K-feldspars, such as the volume of the unit cell as well as the probability of Al cation to occupy one of the T1 sites ($\Sigma t1$).

References

Afouxenidis, D., Polymeris, G.S., Tsirliganis, N.C., Kitis, G., 2012. Computerised curve Deconvolution of TL/OSL curves using a popular spreadsheet program. Radiat. Protect. Dosim. 149, 363–370.

Angeli, V., Kitis, G., Polymeris, G.S., Şahiner, E., Meriç, N., 2019. Component-resolved bleaching correlation between OSL and IRSL signals in various geological materials. Appl. Radiat. Isot. 143, 156–162.

Balian, Eddy, 1977. Figure-of-merit (FOM), an improved criterion over the normalized chi-squared test for assessing goodness-of-fit of gamma-ray spectral peaks. Nucl. Instrum. Methods 145, 389.

Chen, R., Leung, P.L., Stokes, M.J., 2000. Apparent anomalous fading of thermoluminescence with competition with radiationless transitions. Radiat. Meas. 32, 505.

Correcher, V., Garcia-Guinea, J., Delgado, A., 2000. Influence of preheating treatment on the luminescence properties of adularia feldspar (KAlSi3O8), Radiat. Meas 32, 709.

Deer, W.A., Howie, R.A., Zussman, J., 1992. An Introduction to the Rock-Forming Minerals, 2nd ed. Longman, Harlow.

Garcia-Guinea, J., Correcher, V., Delgado, A., Sanchez-Munoz, L., 2003. Cluster linkages between luminescence emission spectra and continuous trap distribution in a volcanic sanidine. Radiat. Meas. 37, 473.

Jain, M., Ankjærgaard, C., 2011. Towards a non-fading signal in feldspar: insight into charge transport and tunnelling from time-resolved optically stimulated luminescence. Radiat. Meas. 46, 292.

Jain, M., Guralnik, B., Andersen, M.T., 2012. Stimulated luminescence emission from localized recombination in randomly distributed defects. J. Phys. Condens. Matter 24, 385402.

Kitis, G., Pagonis, V., 2013. Analytical solutions for stimulated luminescence emission from tunneling recombination in random distributions of defects. J. Lumin. 137, 109.

Kitis, G., Polymeris, G.S., Pagonis, V., Tsirliganis, N.C., 2013. Anomalous fading of OSL signals originating from very deep traps in Durango apatite. Radiat. Meas. 49, 73–81.

Kitis, G., Polymeris, G.S., Sfampa, I.K., Prokic, M., Meriç, N., Pagonis, V., 2016a. Prompt isothermal decay of thermoluminescence in $MgB4_O7$:Dy, Na and $LiB4_O7$:Cu, in dosimeters. Radiat. Meas. Vol. 84, 15–25.

Kitis, G., Polymeris, G.S., Şahiner, E., Meriç, N., Pagonis, V., 2016b. Influence of the infrared stimulation on the optically stimulated luminescence in four K-feldspar samples. J. Lumin. 176, 32–39.

Krbetschek, M.R., Goetze, J., Dietrich, A., Trautmann, T., 1997. Spectral information from minerals relevant for luminescence dating. Radiat. Meas. 27, 695–748.

Kroll, H., Ribbe, P.H., 1987. Determining (Al,Si) distribution and strain in alkali feldspars using lattice parameters and diffraction-peak positions: a review. Am. Mineral. 72, 491.

Larsen, A., Greilich, S., Jain, M., Murray, A.S., 2009. Developing a numerical simulation for fading in feldspar. Radiat. Meas. 44, 467.

Laugier, J.Bochu, B. Graphical powder indexing cell and spacegroup, assignment software. http://www.inpg.gr/LMGP.

Li, B., Li, S.H., 2008. Investigations of the dose-dependent anomalous fading rate of

feldspar from sediments. J. Phys. D Appl. Phys. 41 (22), 225502.
Pagonis, V., Phan, H., Ruth, D., Kitis, G.G., 2013. Further investigations of tunnelling recombination processes in random distributions of defects. Radiat. Meas. 58, 66–74.
Pagonis, V., Jain, M., Thomsen, K.J., Murray, A.S., 2014. On the shape of continuous wave infrared stimulated luminescence signals from feldspars: a case study. J. Lumin. 153, 96–103.
Pagonis, V., Polymeris, G., Kitis, G., 2015. On the effect of optical and isothermal treatments on luminescence signals from feldspars. Radiat. Meas. 82, 93–101.
Polymeris, G.S., Theodosoglou, E., Kitis, G., Tsirliganis, N.C., Koroneos, A., Paraskevopoulos, K.M., 2013. Preliminary results on structural state characterization of K-feldspars by using thermoluminescence. Mediterranean Archaeology Archaeometry 13, 155–161.
Polymeris, G.S., Sfampa, I.K., Niora, M., Stefanaki, E.C., Malletzidou, L., Giannoulatou, V., Pagonis, V., Kitis, G., 2018a. Anomalous fading in TL, OSL and TA-OSL signals of Durango apatite for various grain size fractions; from micro to nano scale. J. Lumin. 195, 216–224.
Polymeris, G.S., Şahiner, E., Aslar, E., Kitis, G., Meriç, N., 2018b. 2018b. Deconvolution of isothermal TA – OSL decay curves from sedimentary quartz using combinations of various contemporary models. Radiat. Meas. 119, 93–101.
Poolton, N.R.J., Ozanyan, K.B., Wallinga, J., Murray, A.S., Bötter-Jensen, L., 2002a. Electrons in feldspar II: a consideration of the influence of conduction band-tail states on luminescence processes. Phys. Chem. Miner. 29, 217.
Poolton, N.R.J., Wallinga, J., Murray, A.S., Bulur, E., Bötter-Jensen, L., 2002b. Electrons in feldspar I: on the wavefunction of electrons trapped at simple lattice defects. Phys. Chem. Miner. 29, 210.
Poolton, N.R.J., Kars, R.H., Wallinga, J., Bos, A.J.J., 2009. Direct evidence for the participation of band-tails and excited-state tunnelling in the luminescence of irradiated feldspars. J. Phys. Condens. Matter 21, 485505.
Şahiner, E., Kitis, G., Pagonis, V., Meriç, N., Polymeris, G.S., 2017. Tunnelling recombination in conventional, post-infrared and post-infrared multi-elevated temperature IRSL signals in microcline K-feldspar. J. Lumin. 188, 514–523.
Sfampa, I.K., Polymeris, G.S., Tsirliganis, N.C., Pagonis, V., Kitis, G., 2014. Prompt isothermal decay of thermoluminescence in an apatite exhibiting strong anomalous fading. Nucl. Instrum. Methods Phys. Res. B 320, 57–63.
Sfampa, I.K., Polymeris, G.S., Pagonis, V., Theodosoglou, E., Tsirliganis, N.C., Kitis, G., 2015. Correlation of basic TL, OSL and IRSL properties of ten K-feldspar samples of various origins. Nucl. Instrum. Methods Phys. Res. B 359, 89–98.
Templer, R.H., 1986. The localised transition model of anomalous fading. Radiat. Protect. Dosim. 17, 493.
Tyler, S., McKeever, S.W.S., 1988. Anomalous fading of thermoluminescence in oligoclase 14, 149.
Visocekas, R., 1985. Tunnelling radiative recombination in labradorite: its association with anomalous fading of thermoluminescence. Nucl. Tracks 10, 521.
Visocekas, R., Geoffry, A., 1977. Tunneling process in afterglow and retrapping of calcite. Phys. Status Solidi 41, 4993.
Visocekas, R., Ceva, T., Marti, C., Lafaucheux, F., Roberts, M.C., 1976;al.,. Tunneling process in afterglow of calcite. Phys. Status Solidi 35, 315.
Wintle, A.G., 1973. Anomalous fading of thermo-luminescence in mineral samples. Nature 245 (5421), 143–144.